Silikáty *28*, s. 289—309 (1984)

Původní práce

POLYTYPISM OF PYROPHYLLITE AND TALC

Part II. Classification and X-ray identification of MDO polytypes

ZDENĚK WEISS, SLAVOMIL ĎUROVIČ*)

Coal Research Institute, 716 07 Ostrava-Radvanice

** Institute of Inorganic Chemistry, Slovak Academy of Sciences, Dúbravská cesta 5, 842 36 Bratislava*

Received 2. 5. 1983

The MDO polytypes of pyrophyllite and talc family have been classified according to their superposition structures into two subfamilies, and according to the YZ projection of their structures into 7 (talc family) and 15 (pyrophyllite family) MDO groups. This geometrical classification which is closely related to the diffraction patterns of these minerals, has been confirmed by systematic calculation of X-ray diffraction patterns for all individual MDO polytypes. These calculations made it also possible to construct identification diagrams for determining the subfamily and the MDO group from the distribution of intensities along the reciprocal rows $\pm 20l$ or $\pm 13l$ and 0 2l, respectively. These two characteristics suffice for the determination of any MDO polytype. The identification is based on visual comparison of single-crystal diffraction patterns with the identification diagrams. A partial identification is possible also using powder diagrams of specimens with random orientation of particles.

INTRODUCTION

Problems related to the classification and X-ray identification of MDO polytypes in some concrete families of phyllosilicates have been analyzed recently in the following works: chlorites [1], [2], Mg-vermiculites [3], micas [4], [5], [6], [7] and kaolinite group [5], [8]. The present paper deals with the classification and X-ray identification of MDO polytypes of pyrophyllite and talc derived in Part I [9] and applies theoretical principles common to all phyllosilicates to this study.

CLASSIFICATION OF MDO POLYTYPES OF PYROPHYLLITE AND TALC

The ideal ditrigonalized model of any polytype of pyrophyllite and talc as defined in Part I [9] implies that its diffraction pattern contains three types of diffractions (orthogonal indexing):

1. diffractions with $h = 3n \wedge k = 3n \wedge h + k = 2n$
2. diffractions with $h \neq 3n \wedge k = 3n \wedge h + k = 2n$
3. remaining diffractions ($h + k = 2n$)

The diffractions of the first type correspond to a fictitious, triperiodic 9-fold average structure (superpositions by $\pm a/3$ and $\pm b/3$, basic vectors $\boldsymbol{a}_1/3$, $\boldsymbol{a}_2/3$, $\boldsymbol{c}_0$; space group $P(\bar{3})12/m$) which is common to all polytypes — no matter whether

periodic or non-periodic — of pyrophyllite and talc, respectively. Therefore also these diffractions are sharp and common to all these polytypes, and useless for their identification.

The diffraction of the second type correspond to a fictitious 3-fold average structure. This structure is identical (for the ideal ditrigonalized model only) to the superposition structure defined according to the OD theory. Such a structure is generated if all possible positions of any OD layer in any polytype of the family are realized simultaneously [10] and its symmetry is obtained by completing any OD grupoid of the family to a group [11]. The superposition structure is by definition triperiodic and thus the corresponding diffractions are always sharp. For the reasons given in the last paragraph of [9], there exist two subfamilies *A* and *B* with different OD symmetries and thus also two superposition structures characteristic for these subfamilies within the respective pyrophyllite or talc families. The superposition structure corresponding to the subfamily A has the symmetry $H_R(\bar{3})12/m$ and basic vectors $\boldsymbol{a}_1$, $\boldsymbol{a}_2$, $3\boldsymbol{c}_0$ (the subscript R means the possibility of selecting a smaller rhombohedral cell). The other superposition structure (B) has the symmetry $H(\bar{3})12/m$ and the basic vectors $\boldsymbol{a}_1$, $\boldsymbol{a}_2$, $\boldsymbol{c}_0$. These symmetries are the same in the talc and in the pyrophyllite family and the corresponding superposition structures (e.g. *A* in both families) differ only in the occupation of the octahedral position containing one Mg atom and 2/3 Al atom, respectively. The above space groups and basic vectors can be easily derived if one takes any polytype of the analyzed subfamily and realizes in a schematic drawing simultaneously all *Z* positions for any of its constituting OD layers (Table IV in [9]). It should only be kept in mind that in the diffraction pattern of a given polytype, the diffractions of its superposition structure acquire diffraction indices related to the lattice geometry of this polytype and not its own lattice geometry given above.

The superposition structure is the first fundamental geometrical characteristics for classification of polytypes. As shown in [1], [7], [12], its symbol can be obtained from the fully descriptive symbol of a polytype in a routine way by an appropriate conversion of the characters. Since the corresponding diffractions are always sharp, the distribution of their intensities can be used to range the polytype — no matter whether periodic or non-periodic — into its appropriate subfamily. It should be emphasized here that all polytypes of the same subfamily have also the same *XZ* projection (common diffractions *h0l*).

The diffractions of the third type are sharp only for periodic polytypes, otherwise they are diffuse. They are characteristic for individual polytypes, but it is not necessary to inspect all of them if a polytype has to be identified, since there are diffractions *0kl* among them and these correspond to the projection of the structure into the *YZ* plane. All polytypes with the same *YZ* projection have also common set of these diffractions. All MDO polytypes within a family can be classified according to their respective *YZ* projection into MDO groups. In a way analogous to that for the superposition structures, also the symbols for *YZ* projections can be determined from the fully descriptive symbols of individual MDO polytypes [1], [7], [12]. As a result, the 10 non-equivalent MDO polytypes of talc derived in [9] were ranged into 7 MDO groups, and the 22 nonequivalent MDO polytypes of pyrophyllite [9] into 15 MDO groups. The *YZ* projection of the structure is the second fundamental geometrical characteristics for the classification of polytypes. Together with the superposition structure it suffices to characterize unambiguously any polytype [7], [12].

A full importance of these facts is evident from a "cross — reference" classification table which can be constructed for any family and which contains in any of its columns the MDO polytypes belonging to the same subfamily, and in any of its rows the MDO polytypes belonging to the same MDO group. It is thus enough to known the distribution of intensities of the selected diffractions of the second and the third types to identify any MDO polytype. The experience has shown that the diffractions $\pm 20l$ or $\pm 13l$ (*2nd* type) and the diffractions $02l$ or $04l$ (*3d* type) are most suitable for these purposes. There is no need to analyze the whole diffraction pattern.

The above considerations refer to the classification of the MDO polytypes within a given family (talc or pyrophyllite). Such a classification, however, can be extended in such a way that it includes also the relations of homomorphy between the polytypes of these two families assigning in general three meso-octahedral pyrophyllite polytypes to one homo-octahedral talc polytype with the same framework of all atoms except those in the octahedral coordination. All these polytypes will have identical or closely related basic vectors, the space group of the homo-octahedral polytype will be their common super-group and their diffraction patterns will also be similar. The assignement of polytypes according to these rules can easily be made if all even and odd orientational characters in the fully descriptive symbols of a meso-octahedral polytype are replaced by the characters *e* and *u*, respectively, leading thus to the corresponding homo-octahedral polytype.

The classification of MDO polytypes of talc and pyrophyllite together with the relations of homomorphy between them is shown in Tab. I. The individual MDO groups of the homo-octahedral family are labelled by Roman numbers I to VII and the meso-octahedral polytypes within any of these groups by Arabic numbers 1 to 3. The individual polytypes in Tab. I labelled by such numbers are represented by their fully descriptive symbols (without enantiomorphous counterparts).

Tab. II shows the same relations as Tab. I. It differs from it only in the form of polytype symbols which are replaced by new indicative symbols suggested for cases when the use of fully descriptive symbols would be too awkward. The new symbols respect the traditional Ramsdell symbolism as well as the new classification based on structural characteristics, and denote unambigously the corresponding polytypes in contrast to the commonly used Ramsdell symbols which do not suffice for these purposes any more. Such a new indicative labelling of polytypes can be made for all phyllosilicates [13]. Any symbol consists, as a rule, of three identifiers: the first one is identical with the traditional Ramsdell symbol, the second — as a subscript — denotes the subfamily, and the third, following after a hyphen (—) is a combination of the numbers of the appropriate MDO groups, separated by dashes (,). There is one or two such numbers for homo- and meso-octahedral polytypes, respectively. E.g. the symbol $1M_A$-I denotes a talc polytype with the fully descriptive symbol $\left|\begin{smallmatrix} e\,.\,e \\ 3\;\;3 \end{smallmatrix}\right|$, $1Tc_A$-II, 1 denotes a pyrophyllite polytype with the symbol $\left|\begin{smallmatrix} 2\,.\,2 \\ 5\;\;1 \end{smallmatrix}\right|$, etc. Such a complete indicative designation of polytypes can be simplified in cases when some of the identifiers are redundant. The hierarchy of the importance of the individual identifiers is determined according to their sequence (see Tab. II where the non-redundant indicative symbols are given in parentheses).

Table I

Classification table of MDO polytypes of talc and pyrophyllite.
Full symbols of MDO polytypes are given in the respective lines

Sub-family	*A*			*B*		
MDO group	homo-octahedral	MDO group	meso-octahedral	homo-octahedral	MDO group	meso-octahedral
I	$\left\vert \begin{matrix} e.e \\ 3\ 3 \end{matrix} \right\vert$	1	$\left\vert \begin{matrix} 0.0 \\ 3\ 3 \end{matrix} \right\vert$	$\left\vert \begin{matrix} e.e \\ 3\ 0 \end{matrix} \right\vert$	1	$\left\vert \begin{matrix} 0.0 \\ 3\ 0 \end{matrix} \right\vert$
		2	$\left\vert \begin{matrix} 2.4 \\ 3\ 3 \end{matrix} \right\vert$		2	$\left\vert \begin{matrix} 2.4 \\ 3\ 0 \end{matrix} \right\vert$
		3	$\left\vert \begin{matrix} 5.1\ 1.5 \\ 0\ 0\ 0\ 0 \end{matrix} \right\vert$		3	$\left\vert \begin{matrix} 5.1\ 1.5 \\ 0\ 3\ 0\ 3 \end{matrix} \right\vert$
II	$\left\vert \begin{matrix} e.e \\ 5\ 1 \end{matrix} \right\vert$	1	$\left\vert \begin{matrix} 2.2 \\ 5\ 1 \end{matrix} \right\vert$	—		—
III				$\left\vert \begin{matrix} e.e \\ 5\ 4 \end{matrix} \right\vert$	1	$\left\vert \begin{matrix} 2.2 \\ 5\ 4 \end{matrix} \right\vert$
IV	$\left\vert \begin{matrix} u.u\ u.u \\ 0\ 4\ 0\ 2 \end{matrix} \right\vert$	1	$\left\vert \begin{matrix} 3.3\ 3.3 \\ 0\ 4\ 0\ 2 \end{matrix} \right\vert$	$\left\vert \begin{matrix} u.u\ u.u \\ 0\ 1\ 0\ 5 \end{matrix} \right\vert$	1	$\left\vert \begin{matrix} 3.3\ 3.3 \\ 0\ 1\ 0\ 5 \end{matrix} \right\vert$
		2	$\left\vert \begin{matrix} 1.5\ 5.1 \\ 0\ 4\ 0\ 2 \end{matrix} \right\vert$		2	$\left\vert \begin{matrix} 5.1\ 1.5 \\ 0\ 1\ 0\ 5 \end{matrix} \right\vert$
		3	$\left\vert \begin{matrix} 5.1\ 1.5 \\ 0\ 4\ 0\ 2 \end{matrix} \right\vert$		3	$\left\vert \begin{matrix} 1.5\ 5.1 \\ 0\ 1\ 0\ 5 \end{matrix} \right\vert$
V	$\left\vert \begin{matrix} u.u\ u.u \\ 2\ 0\ 4\ 0 \end{matrix} \right\vert$	1	$\left\vert \begin{matrix} 5.5\ 1.1 \\ 2\ 0\ 4\ 0 \end{matrix} \right\vert$	$\left\vert \begin{matrix} u.u\ u.u \\ 2\ 3\ 4\ 3 \end{matrix} \right\vert$	1	$\left\vert \begin{matrix} 5.5\ 1.1 \\ 2\ 3\ 4\ 3 \end{matrix} \right\vert$
VI	$\left\vert \begin{matrix} e.e\ e.e\ e.e \\ 3\ 1\ 5\ 3\ 1\ 5 \end{matrix} \right\vert$	1	$\left\vert \begin{matrix} 0.0\ 2.2\ 4.4 \\ 3\ 1\ 5\ 3\ 1\ 5 \end{matrix} \right\vert$			
		2	$\left\vert \begin{matrix} 2.4\ 4.0\ 0.2 \\ 3\ 1\ 5\ 3\ 1\ 5 \end{matrix} \right\vert$	—		—
		2		—		—
		3	$\left\vert \begin{matrix} 4.2\ 0.4\ 2.0 \\ 3\ 1\ 5\ 3\ 1\ 5 \end{matrix} \right\vert$			
VII	—		—	$\left\vert \begin{matrix} e.e\ e.e\ e.e \\ 3\ 4\ 5\ 0\ 1\ 2 \end{matrix} \right\vert$	1	$\left\vert \begin{matrix} 0.0\ 2.2\ 4.4 \\ 3.4\ 5\ 0\ 1\ 2 \end{matrix} \right\vert$
					2	$\left\vert \begin{matrix} 2.4\ 4.0\ 0.2 \\ 3\ 4\ 5\ 0\ 1\ 2 \end{matrix} \right\vert$
					3	$\left\vert \begin{matrix} 4.2\ 0.4\ 2.0 \\ 3\ 4\ 5\ 0\ 1\ 2 \end{matrix} \right\vert$

Table II

Classification table of MDO polytypes of talc and pyrophyllite. New indicative symbols of MDO polytypes are given in the respective lines (non-redundant symbols are given in parentheses)

Sub-family	*A*			*B*		
MDO group	homo-octahedral	MDO group	meso-octahedral	homo-octahedral	MDO group	meso-octahedral
I	$1M_A$ — I ($1M_A$)	1 2 3	$1M_A$ — I, 1 ($1M_A$ — 1) $1M_A$ — I, 2 ($1M_A$ — 2) $2M_A$ — I, 3	$1M_B$ — I ($1M_B$)	1 2 3	$1M_B$ — I, 1 ($1M_B$ — 1) $1M_B$ — I, 2 ($1M_B$ — 2) $2M_B$ — I, 3
II	$1Tc_A$ — II ($1Tc_A$)	1	$1Tc_A$ — II, 1 ($1Tc_A$ — 1)	—		—
III	—		—	$1Tc_B$ — III ($1Tc_B$)	1	$1Tc_B$ — III, 1 ($1Tc_B$ — 1)
IV	$2M_A$ — IV	1 2 3	$2M_A$ — IV, 1 $2M_A$ — IV, 2 $2M_A$ — IV, 3	$2M_B$ — IV	1 2 3	$2M_B$ — IV, 1 $2M_B$ — IV, 2 $2M_B$ — IV, 3
V	$2M_A$ — V	1	$2M_A$ — V, 1	$2M_B$ — V	1	$2M_B$ — V, 1
VI	$3T_A$ — VI ($3T_A$)	1 2 3	$3T_A$ — VI, 1 ($3T_A$ — 1) $3T_A$ — VI, 2 ($3T_A$ — 2) $3T_A$ — VI, 3 ($3T_A$ — 3)	—		—
VII				$3T_B$ — VII ($3T_B$)	1 2 3	$3T_B$ — VII, 1 ($3T_B$ — 1) $3T_B$ — VII, 2 ($3T_B$ — 2) $3T_B$ — VII, 3 ($3T_B$ — 3)

X-RAY IDENTIFICATION OF POLYTYPES OF TALC AND PYROPHYLLITE

From the classification of polytypes carried out in the previous paragraph it follows that in order to identify any MDO polytype it suffices to determine its subfamily and its MDO group. Nevertheless, the identification may be complicated by the fact that the diffraction patterns of talc polytypes are very similar to analogous pyrophyllite polytypes and it is therefore advisable to determine the family first, using also other than X-ray methods (e. g. chemical analysis). Besides, it is known that homo-octahedral talc has its lattice geometry slightly different from that of meso-octahedral pyrophyllite so that in their respective powder diagrams the coinciding diffractions 060, $\bar{3}\bar{3}1$ and $\bar{3}31$, yield a diffraction peak at 0.1495 nm and at 0.1529 nm in pyrophyllite and talc (*1Tc*), respectively.

The identification of a polytype within a family is influenced also by the experimental technique used, and according to it is possible to perform the idenfitication at various levels using:

a) single-crystal data obtained by the refinement of the structure of a particular polytype,

b) visual comparison of the distribution of intensities of selected diffractions obtained by single-crystal technique with calculated identification diagrams,

c) special preparation techniques of a polycrystalline sample, special methods of recording the diffraction pattern and comparison of experimental diffraction pattern with the calculated patterns with respect to the corresponding techniques. In this context *e.g.* powder diffraction method using specimens with removed texture or oblique texture method in electron diffraction [14], [15] and X-ray diffractometry [16], [17] can be mentioned.

The "resolwing power" of these methods of investigation and therefore also the quality of the results thus obtained differ considerably. The choice of a particular approach depends on the formulation of the concrete problem, i.e. on the amount and quality of the information which we wish to obtain, but also on the accessible experimental technique and on the nature of the investigated samples. E.g. a higher degree of disorder may cause the diffractions of the third type to be smeared out into continuous streaks without well-developed maxima, so that it makes no sense to attempt to identify a particular polytype and only a determination of the subfamily is possible.

The aim of the present paper is to identify MDO polytypes and therefore we exclude the complete structure analysis as mentioned in a) from our further considerations and concentrate upon the points b) and c), i.e. on the determination of identification criteria of the MDO polytypes derived in [9]. From the classification presented in the previous paragraph it is known what types of diffractions have the same distribution of intensities within a subfamily or within an MDO group, and it was now necessary to determine concrete values of these distributions. For this purpose we have performed systematic calculations of theoretical diffraction patterns of individual MDO polytypes using a special computer program DIFP. As a side effect of such calculations we have expected a verification of our classification scheme. The calculations consisted of an automatic generation of the coordinates of all atoms within the unit cell of a polytype using the atomic coordinates within an OD packet in its standard orientation, and the fully descriptive symbol of the considered polytype. The effect of the ditrigonalization was not taken into consideration since our experience [1], [3] has shown that is has

Table III

Lattice parameters of the individual MDO polytypes used for calculation of their diffraction patterns. Equations for calculation of l_o indices (corresponding to the six-layer orthogonal cell) with respect to the different types of lattice geometry are given in the last column. The h_r, kr and l_r indices correspond to the lattice geometry of individual MDO polytype.

Family	Type of lattice	Polytype	*a* (nm)	*b* (nm)	*c* (nm)	α (°)	β (°)	γ (°)	Transformation of indices
Talc	*a*	$1M_B$ — I	0.5293	0.9179	0.9381	90	90	90	$l_o = 6l_r$
	b	$2M_B$ — IV; $2M_B$ — V	0.5293	0.9179	1.8762	90	90	90	$l_o = 3l_r$
	c	$3T_A$ — VI; $3T_B$ — VII	0.5293	0.5293	2.8143	90	90	120	$l_o = 2l_r$
	d	$1M_A$ — I; $1Tc_A$ — II	0.5293	0.9179	0.9545	90	100.6	90	$l_o = 6l_r + 2h_r$
	e	$1Tc_B$ — III	0.5293	0.9179	0.9867	108.1	90	90	$l_o = 6l_r + 2k_r$
	f	$2M_A$ — IV; $2M_A$ — V	0.5293	0.9179	1.9090	90	100.6	90	$l_o = 3l_r + h_r$
Pyrophyllite	*a*	$1M_B$ — I, 1; $1M_B$ — I, 2	0.5160	0.8966	0.9190	90	90	90	$l_o = 6l_r$
	b	$2M_B$ — I, 3; $2M_B$ — IV, 1 $2M_B$ — IV, 2; $2M_B$ — IV, 3 $2M_B$ — V, 1	0.5160	0.8966	1.8380	90	90	90	$l_o = 3l_r$
	c	$3T_A$ — VI, 1; $3T_A$ — VI, 2 $3T_A$ — VI, 3 $3T_B$ — VII, 1; $3T_B$ — VII, 2 $3T_B$ — VII, 3	0.5160	0.5160	2.7570	90	90	120	$l_o = 2l_r$
	d	$1M_A$ — I, 1; $1M_A$ — I, 2 $1Tc_A$ — II, 1	0.5160	0.8966	0.9350	90	100.6	90	$l_o = 6l_r + 2h_r$
	e	$1Tc_B$ — III, 1	0.5160	0.8966	0.9663	108.6	90	90	$l_o = 6l_r + 2k_r$
	f	$2M_A$ — I, 3; $2M_A$ — IV, 1 $2M_A$ — IV, 2; $2M_A$ — IV, 3 $2M_A$ — V, 1	0.5160	0.8966	1.8700	90	100.6	90	$l_o = 3l_r + h_r$

no significant influence on the distribution of intensities. The following chemical composition was assumed:

$Mg_3(Si_4O_{10})(OH)_2$ for talc and

$Al_2(Si_4O_{10})(OH)_2$ for pyrophyllite.

The lattice parameters used are given in Tab. III.

Identification of polytypes from data obtained by single-crystal diffraction

As we have already stated, the distribution of intensities of $\pm 20l$ or $\pm 13^l$ diffractions may be used with advantage for identification of the subfamily. Calculated values $|F|^2$ of the above characteristic diffractions corresponding to subfamily A and B for talc and pyrophyllite are shown in Figs. 1 and 2 for purposes of visual comparison with observed diffraction patterns. The indexing refers to an orthogonal six-layer cell $\boldsymbol{a}$, $\boldsymbol{b}$, $6\boldsymbol{c}_0$ which is the smallest C-centered common supercell for all MDO polytypes. Equations for calculation of l_0 indices (corresponding to the six-layer orthogonal cell) with respect to the different types of lattice geometry are given in Tab. III. The subfamily A can be immediately recognized by

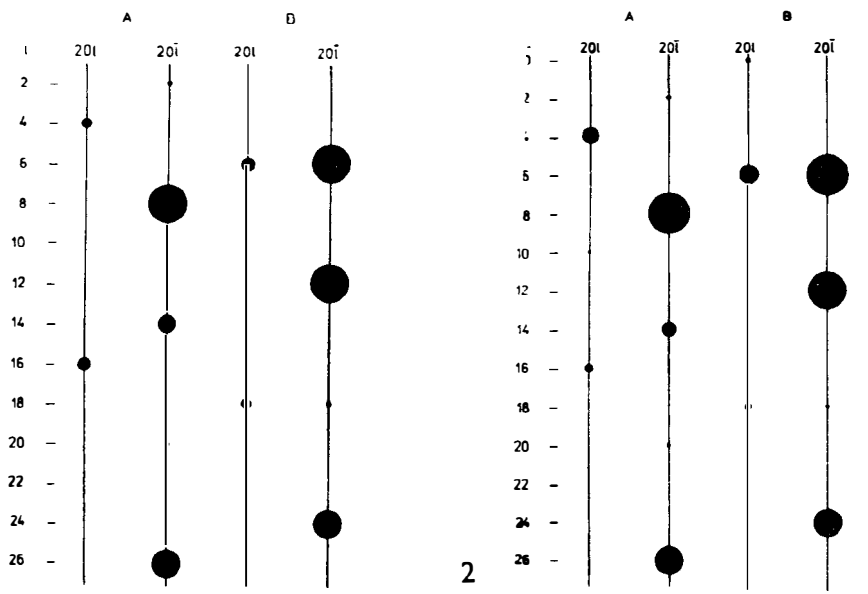

Fig. 1. Visual representation of calculated $|F|^2$ values (the strongest $|F|^2$ value of each subfamily is drawn as the biggest circle) for charateristic diffractions 20l of MDO polytypes of talc and their classification into the subfamilies A and B. The indexing refers to an ortohogonal six-layer cell. For calculation of indices the equations corresponding to d) type of lattice for subfamily A and a) type of lattice for subfamily B were used (see Tab. III).

Fig. 2. Visual representation of calculated $|F|^2$ values (the strongest $|F|^2$ value of each subfamily is drawn as the biggest circle) for characteristic diffractions 20l of MDO polytypes of pyrophyllite and their classification into the subfamilies A and B. The indexing refers to an orthogonal six-layer cell. For calculation of indices the equations corresponding to d) type of lattice for subfamily A and a) type of lattice for subfamily B were used (see Tab. III).

extinctions due to its rhombohedral superposition structure*). Let us just recall that due to the Laue symmetry $\bar{3}m$ corresponding to the superposition structures in both A and B subfamilies, the distribution of intensities along the reciprocal rows $20l_0$, $\bar{1}3l_0$, $1\bar{3}l_0$, $20\bar{l}_0$, $\bar{1}3\bar{l}_0$ and $1\bar{3}\bar{l}_0$ are the same.

The diagrams of $|F|^2$ values corresponding to $02l$ diffractions for identification of MDO groups of both families are shown in Figs. 3 to 7. For homo-octahedral family (talc), these groups are denoted in the same way as in Tab. I, i.e. I to VII. The designations is analogous for meso-octahedral family (pyrophyllite), i.e. I, 1; I, 2; I, 3; etc.

As it may be deduced from the diagrams quoted above, the distinction of subfamilies is possible using the proposed visual comparison (Figs. 1 and 2). However, the $20l$ diffractions do not suit for distinction of the families. Within a family, the visual techniques is suitable for the distinction of the MDO groups from the distribution of the intensities of $02l$ diffractions. Our calculations revealed however that the complete diffraction patterns of the MDO polytypes $3T_A$-VI,1 and

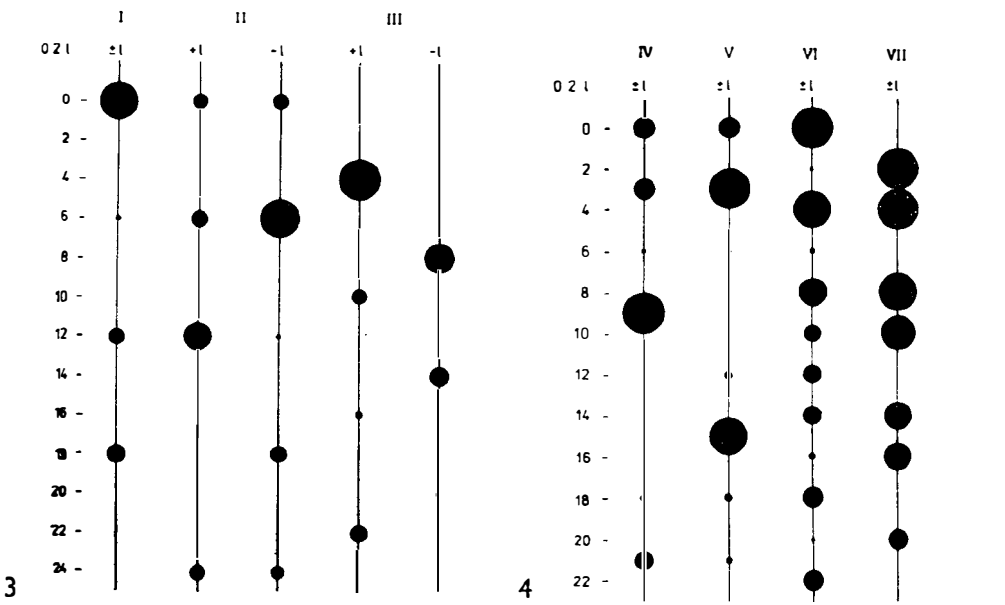

Fig. 3. Visual representation of calculated $|F|^2$ values (the strongest $|F|^2$ value of each MDO group is drawn as the biggest circle) for characteristic diffractions $02l$ of MDO polytypes of talc and their classification into the MDO groups I, II and III. The indexing refers to an orthogonal six-layer cell. The equations for calculation of indices are given in Tab. III.

Fig. 4. Visual representation of calculated $|F|^2$ values (the strongest $|F|^2$ value od each MDO group is drawn as the biggest circle) for characteristic diffractions $02l$ of MDO polytypes of talc and their classification into the MDO groups IV to VII. The indexing refers to an orthogonal six-layer cell. The equations for calculation of indices are given in Tab. III.

*) Zvyagin [15] refers this superposition structure to an one — layer monoclinic cell a, $b/3$ c_0—$a/3$ which — but only by its geometry — corresponds evidently to one third of the correct cell.

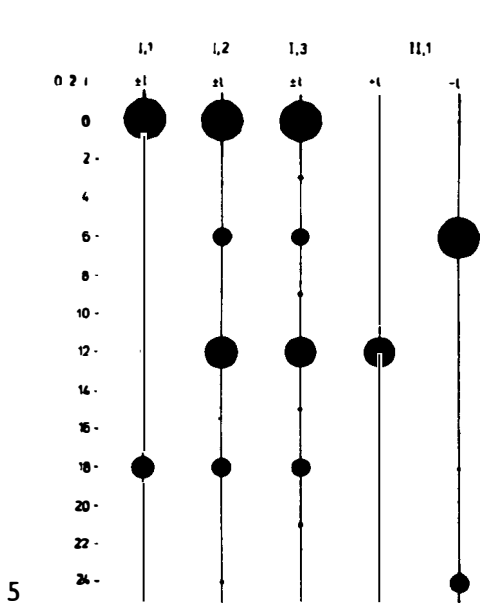

5

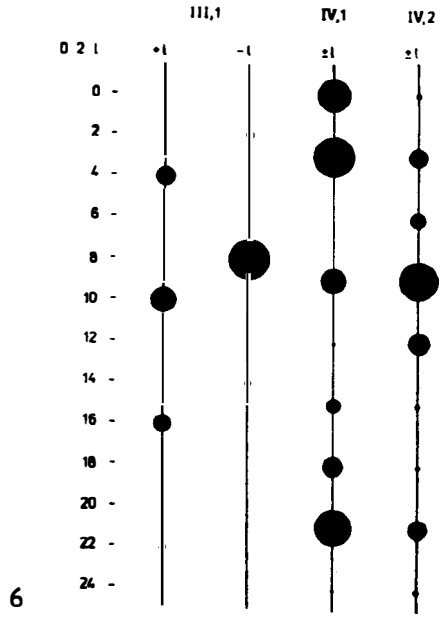

6

Fig. 5. Visual representation of calculated $|F|^2$ values (the strongest $|F|^2$ value of each MDO group is drawn as the biggest circle) for characteristic diffractions 02l of MDO polytypes of pyrophyllite and their classification into the MDO groups I, 1; I, 2; I, 3; II, 1. The indexing refers to an orthogonal six-layer cell. The equations for calculation of indices are given in Tab. III.

Fig. 6. Visual representation of calculated $|F|^2$ values (the strongest $|F|^2$ value of each MDO group is drawn as the biggest circle) for characteristic diffractions 02l of MDO polytypes of pyrophyllite and their classification into the MDO groups III, 1; IV, 1 and IV, 2. The indexing refers to an orthogonal six-layer cell. The equations for calculation of indices are given in Tab. III.

$3T_A$-VI,3 are so similar that their visual distinction is impossible. The same holds for the MDO polytypes $3T_B$-VII, 1; $3T_B$-VII, 2 and $3T_B$-VII, 3 (see Fig. 7). However, there will be difficulties if we try to use the distribution of the intensities of 02*l* diffractions also for the distinction of the families, e.g. for the distinction of MDO groups I (talc-family) and I, 2 (pytophyllite-family). In some cases, the distinction of MDO groups (within a family) can be very difficult if the influence of stacking disorder or desymmetrization of structure will be considered. Fortunately, it turned out that the desymmetrization of the structure caused minor changes in the distribution of the intensities of 02*l* diffractions but major changes in the distribution of the intensities of $\pm$ 20*l* diffractions. These changes were found to be more pronounced in pyrophyllite than in the talc. If we take the ditrigonalization of the tetrahedral sheet as a "measure" of the desymmetrization of the structure we may explain the above changes by the magnitude of the angle of rotation of the tetrahedra. In pyrophyllite, this angle $\alpha = 10 . 2°$ [18] and in talc [19] $\alpha = 3 . 4°$. The above mentioned facts are evident from a comparison of theoretical $|F|^2$ values calculated for the structure of $1Tc_A$-II,1 and $1Tc_A$-II polytypes with an idealized symmetry and the $|F|^2$ values obtained from the structure analysis of real samples [18], [19] as shown in Figs. 8 and 9.

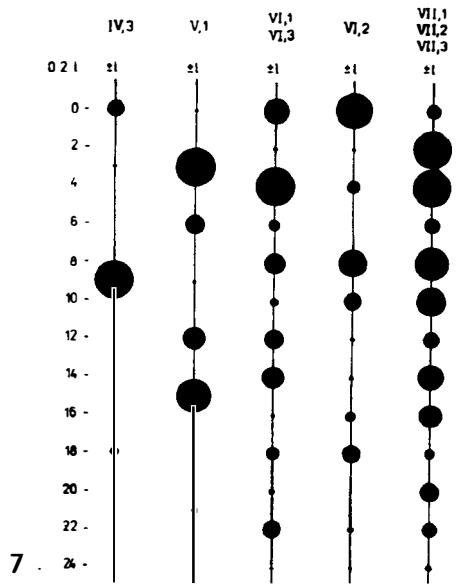

7

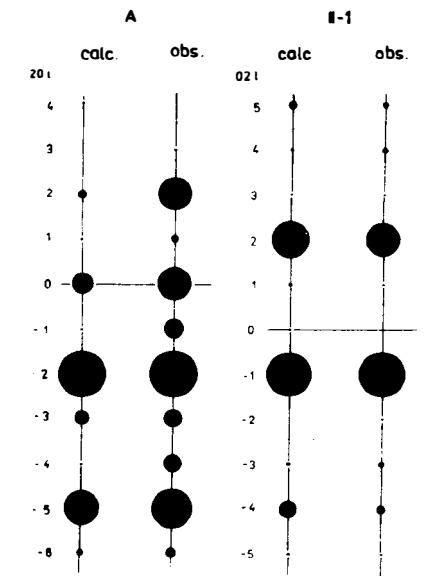

8

Fig. 7. Visual representation of calculated | F |² values (the strongest | F |² value of each MDO group is drawn as the biggest circle) for characteristic diffractions 02l of MDO polytypes of pyrophyllite and their classification into the MDO groups IV, 3; V, 1; VI, 1 (VI, 3); VI, 2 and VII, 1 (VII, 2; VII, 3). The indexing refers to an orthogonal six-layer cell. The equations for calculation of indices are given in Tab. III.

Fig. 8. Comparison of the characteristic | F(20l) |² and | F(02l) |² values calculated from the structure data of Lee and Guggenheim [18] — (obs) with the theoretical values calculated for MDO polytype $1Tc_A$ — II, 1 of pyrophyllite — (calc). | F |² values are normalized to the strongest diffraction. The indexing refers to actual one-layer cell.

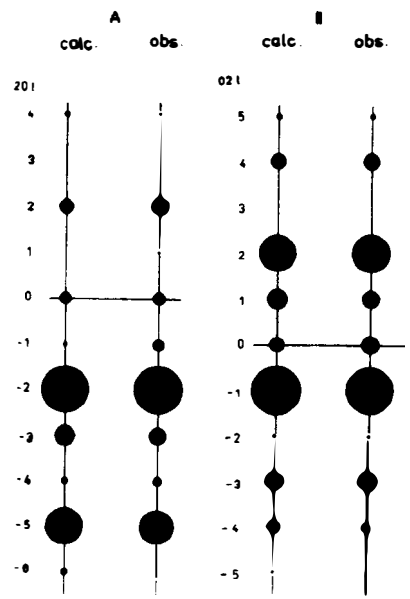

Fig. 9. Comparison of the characteristic | F(20l) |² and | F(02l) |² values calculated from the structure data of Rayner and Brown [19] — (obs) with the theoretical values calculated for MDO polytype $1Tc_A$ — II of talc — (calc) . | F |² values are normalized to the strongset diffraction. The indexing refers to actual one-layer cell.

Table IV

Calculated X-ray powder diffraction patterns of MDO polytypes of pyrophyllite belonging to subfamily *A*. The calculated intensity of diffraction lines corresponds to the analysis of the sample with random oriented particles. The values of relative intensities of diffraction lines are indicated in the lines corresponding to interplanar spacing *d*.

d (nm)	$1M_A$ — I, 1 $3T_A$ — VI, 2	$1M_A$ — I, 2 $3T_A$ — VI, 1 $3T_A$ — VI, 3	$1Tc_A$ — II, 1	$2M_A$ — IV, 1	$2M_A$ — IV, 2	$2M_A$ — IV, 3	$2M_A$ — V, 1	$2M_A$ — I, 3
0.919	59	47	59	60	59	56	58	50
0.916								
0.459	43	31	38	39	38	39	38	33
0.458								
0.448	100	40						42
0.447				42				
0.446					54	100	45	
0.441			87					
0.436				62	34		61	
0.435								
0.434								
0.425	45	100	66	21	63		62	100
0.415							18	
0.414				95	58	24		
0.403	2	24	73		23		22	21
0.402								
0.397								
0.389					7	21	49	5
0.375	88	30	14	23	3	23	3	28
0.362				21	42	68	2	4
0.361								
0.347	42	12	24	11		11		9
0.341					1			
0.334				5		2	32	4
0.321	7	26	32	3	18	3	18	25
0.320								
0.307				91				
0.306	67	54	68		80	68	66	58
0.305								
0.296	8	23	24	3	16	3	16	23
0.294								
0.290							2	
0.284				5	1	1	18	2
0.273	15	4	12	4		4		3
0.263				6	13	22	3	2
0.258								
0.254	58	40	46	49	45	46	45	42
0.253								
0.249								
0.248								
0.242	100	80	100	100	100	95	100	84
0.235		5	13		6		6	4
0.234	3			3		3		
0.230	4	3	5	5	5	4	4	4
0.227				12	6	3	3	2

Continuing Tab. IV

d (nm)	$1M_A$ — I, 1 $3T_A$ — VI, 2	$1M_A$ — I, 2 $3T_A$ — VI, 1 $3T_A$ — VI, 3	$1Tc_A$ — II, 1	$2M_A$ — IV, 1	$2M_A$ — IV, 2	$2M_A$ — IV, 3	$2M_A$ — V, 1	$2M_A$ — I, 3
0.225		4		6				4
0.223		3	5		5		6	
0.222						3		
0.221	7			3				
0.219		12	9		10	9	9	12
0.218								
0.217								
0.216	27	21	26	26	26	25	26	23
0.213		3	6		4		4	
0.211				9	4		5	2
0.207	14	15	17	14	16	13	16	15
0.204			7	7	4		3	
0.201		2	5		2		2	1
0.198					3	6	5	1
0.194	8	2	1	2		2		2
0.192	3			4				3
0.191					4	8		
0.189		4			4		4	4
0.188	13		5	4		4		
0.186					3	5		
0.184	8	7	9	9	8	9	11	7
0.181		3	6		3		3	3
0.180	2							
0.177				7	4	2		
0.175				3	1		2	
0.174	2	5	4		3		3	5
0.172								
0.171								
0.170		4		3			5	4
0.169	11		9		7	9		
0.168		10	9	10	10		11	11
0.167	4			12		4		
0.166		4	10		5		9	4
0.164	33	23	28	29	29	30	27	24
0.163								
0.162	8	3	5					3
0.161	8	4	3		2	3		4
0.160				4			6	
0.159	2	5	6		4		4	5
0.157	2	2	3	9	7	6	7	2
0.156	2	5	5		4		4	4

When making the refinement of the structure of investigated polytypes — which is the best identification possible — the calculated values of structure factors based on the ideal model may be used with advantage as initial models. These values corresponding to individual MDO polytypes are available on request from the present authors.

Table V

Calculated X-ray powder diffraction patterns of MDO polytypes of pyrophyllite belonging subfamily *B*. The calculated intensity of diffraction lines corresponds to the analysis of the sample with random oriented particles. The values of relative intensities of diffraction lines are indicated in the lines corresponding to interplanar spacing *d*

d (nm)	$1M_B$—I, 1 $1M_B$—I, 2	$1Tc_B$—III, 1	$2M_B$—IV, 1 $2M_B$—IV, 3	$2M_B$—IV, 2 $2M_B$—V, 1	$2M_B$—I, 3	$3T_B$—VII, 1 $3T_B$—VII, 2 $3T_B$—VII, 3
0.919	42		45	52	48	49
0.916		60				
0.459	30		29	37	33	32
0.458		39				
0.448	71		25		71	
0.447				37		
0.446						
0.441		94				71
0.436						
0.435			100	100	20	
0.425		86				62
0.415						
0.414						
0.403				45		
0.402	100		28		100	19
0.397		2				
0.389						
0.377		50				41
0.375						
0.362				56		
0.361			57		10	
0.347		35				31
0.341						
0.334						
0.321				23	49	
0.320	48		14			10
0.307						
0.306	48		51	59	54	56
0.305		68				
0.296						19
0.294		24				
0.290						
0.284			25	24	5	
0.273		15				13
0.263						
0.258	5	7	5	6	6	6
0.254						
0.253	25		11	17	25	
0.249	81		86	100	93	
0.248		100				100
0.242						
0.235						8
0.234		12				
0.230	4	7	5	6	5	5
0.227						
0.225	43	45	48	56	49	52
0.223						
0.222			8			
0.221						5

Continuing Tab. V

d (nm)	$1M_B$—I, 1 $1M_B$—I, 2	$1Tc_B$—III, 1	$2M_B$—IV, 1 $2M_B$—IV, 3	$2M_B$—IV, 2 $2M_B$—V, 1	$2M_B$—I, 3	$3T_B$—VII, 1 $3T_B$—VII, 2 $3T_B$—VII, 3
0.219		8				7
0.218	6		2			
0.217				5	5	5
0.216						
0.213		5				3
0.211			5	4	2	
0.207		4				3
0.204	8		2	5	8	3
0.201	7		2	4	6	3
0.198	8	1 2	8	9	9	9
0.194		5				4
0.192		5				3
0.191			5	5	1	
0.189		3				
0.188		3				3
0.186			5	4	2	
0.184	6	6	8	8	7	7
0.181	6	2	3	3	6	
0.180		3				3
0.177						
0.175						
0.174		5				4
0.172	14	10	16	18	16	17
0.171		12				
0.170	5		8	9	7	
0.169	7	10	9	10	7	8
0.168		10				8
0.167	11		4			6
0.166		5		5	10	
0.164		7				5
0.163			7	7	2	
0.162		6				5
0.161						
0.160	6	2	2	3	6	
0.159	8		2	4	7	2
0.157			2	2	1	
0.156		3				
0.155		4				4

Identification of polytypes using powder diffraction

Using the powder diffraction methods, the identification of polytypes becomes much more complicated than the identification based on single-crystal data. Even supposing that a sample with random orientation of particles could be prepared for the X-ray analysis (for reflexion or transmission techniques) and that the different polytypes will not be mixed in the sample, an unambiguous identification of all MDO polytypes will be impossible. As deduced from calculations of powder diffraction patterns performed using the DIFK program [20] for random orientation of particles, a powder diffraction patterns contains, in addition to

Table VI.

Calculated X-ray powder diffraction patterns of MDO polytypes of talc. The calculated intensity of diffraction lines corresponds to the analysis of the sample with random oriented particles The values of relative intensities of diffraction lines are indicated in the lines corresponding to interplanar spacing *d*

d (nm)	$1M_A$—I $3T_A$—VI	$1Tc_A$—II	$2M_A$—IV	$2M_A$—V	$1M_B$—I	$1Tc_B$—III $3T_B$—VII	$2M_B$—IV $2M_B$—V
0.938	99	99	99	96	100	100	100
0.469	17	16	16	16	19	15	16
0.459	44				64		21
0.457			45	37			
0.453		61				61	
0.446			23	42			86
0.436	66	23	12	21		55	
0.425			40	12			
0.412	10	41	5	4	90		23
0.398			5	36			
0.384	36	18	10	10		37	
0.370			31	2			48
0.356	14	21	4	4		28	
0.342				24			
0.328	15	15	5	5	43		11
0.313	63	63	69	61	64	64	64
0.302	15	10	5	5		18	
0.290			1	13			21
0.279	4	10	1	2		12	
0.268			10	2			
0.264	11	11	11	10			
0.260	27	25	25	24			
0.258					25		
0.255					100	99	99
0.248	100	100	100	100			
0.240	2	7				7	
0.235	2	2	2	2			
0.232			5				
0.231				2	66	66	70
0.229	2	2	2				
0.228				3			
0.226	3	2					
0.223	11				5	6	2
0.221	30	30	30	30			
0.218		4				3	
0.216			4	4			
0.215							4
0.212	18	17	17	17		3	
0.209		5			7		2
0.206		3			6		2
0.202			2	3	16	16	16
0.199	3	2	1	1		4	
0.196	4	1	4	1		3	4
0.193	7	7	6	6			
0.192						3	

strong diffractions $\pm 20l$, $\pm 13l$, $02l$ (which are decisive for the identification of polytypes according to the above mentioned classification), also strong diffractions $00l$ and $\pm 11l$. The latter overlap the former to such an extent that the distinction of some polytypes by means of powder diffraction method is practically impossible, i.e. these polytypes have the same diffraction powder pattern. From the above calculations it follows that the following MDO polytypes have the undistinguishable powder diffraction patterns:

a) MDO polytypes of talc:

$1M_A$-I and $3T_A$-VI; $1Tc_B$-III and $3T_B$-VII;

$2M_B$-IV and $2M_B$-V

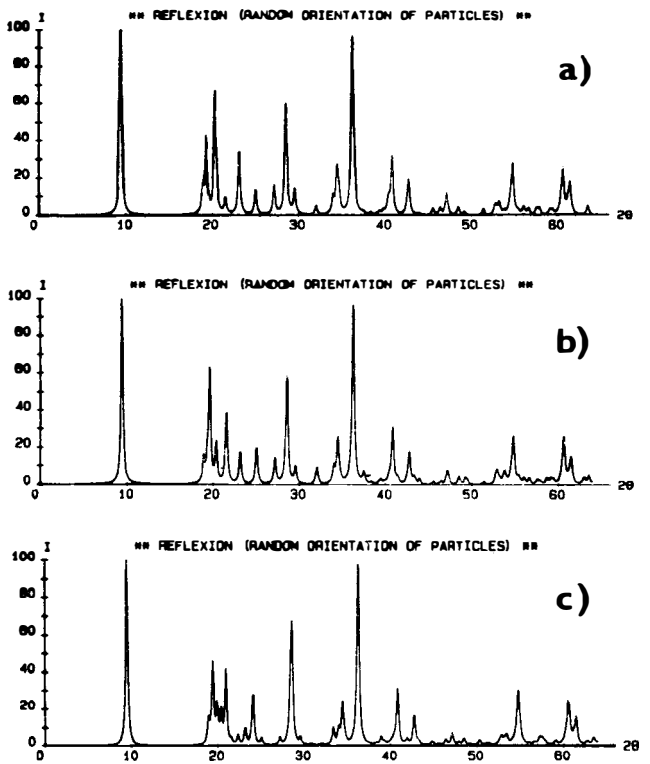

Fig. 10. Calculated X-ray powder diffraction patterns of three MDO polytypes of talc (experimental arrangement: diffractometer, Cu radiation, random orientation of particles in the sample):

a) $\left|\begin{matrix} e\,.\,e \\ 3\;\;3 \end{matrix}\right|$ $(1M_A - I)$

b) $\left|\begin{matrix} e\,.\,e \\ 5\;\;1 \end{matrix}\right|$ $(1Tc_A - II)$

c) $\left|\begin{matrix} u\,.\,u\,.\,u\,.\,u \\ 0\;\;4\;\;\bullet\;\;2 \end{matrix}\right|$ $(2M_A - IV)$

b) MDO polytypes of pyrophyllite:

$1M_A$-I, 1 and $3T_A$-VI, 2; $1M_A$-I, 2 and $3T_A$-VI, 1 and $3T_A$-VI, 3;
$3T_A$-VI, 1 and $3T_A$-VI, 3; $1M_B$-I, 1 and $1M_B$-I, 2;
$2M_B$-VI, 1 and $2M_B$-IV, 3; $2M_B$-IV, 2 and $2M_B$-I, 3;
$3T_B$-VII, 1 and $3T_B$-VII, 2 and $3T_B$-VII, 3.

This fact may be also deduced from Tables IV, V and VI where calculated intensities of diffraction lines are given together with their interplanar spacings for individual MDO polytypes of talc and pyrophyllite. As shown in the tables, the distinction of MDO polytypes belonging to the *A* subfamily from polytypes belonging to *B* subfamily is possible using the method of powder diffraction. However, the distinction of polytypes within a subfamily is not unambiguous. In some polytypes, the differences in the theoretical diffraction patterns are small and even supposing that the experiment was performed with high accuracy, their distinction can not be guaranteed. MDO polytypes $1M_A$-I, 2 and $2M_A$-I, 3 of pyrophyllite may be quoted as an example of it. The point is whether the identification of polytypes may be based on a not very pronounced difference of intensity in one or two diffraction lines, particularly if we take into account that real structure of the investigated sample or other influences associated with the preparation of the sample could alter the observed diffraction pattern. For example, if we consider as sufficient for the distinction of MDO polytypes of talc $1M_A$-I, $1Tc_A$-II and $2M_A$-IV the differences of intensities of a number of diffraction lines (in the angles from 18.8 to 27.3° $2\Theta_{CuK\alpha}$), then we can make the distinction within this limitation. Calculated powder diffraction patterns of these polytypes are shown in Fig. 10.

Nevertheless, when applying the proposed identification diagrams in the practice, we must bear in mind that these diagrams were deduced from an idealized symmetry of structures. Therefore, we must decide to our own discretion, whether such differences are sufficient for identification of polytypes with respect to our experimental technique.

References

[1] Weiss Z., Ďurovič S.: Acta Cryst. *B39*, 552 (1983).
[2] Ďurovič S., Dornberger-Schiff K., Weiss Z.: Acta Cryst. *B39*, 547 (1983).
[3] Weiss Z., Ďurovič S.: Acta Cryst. *A36*, 633 (1980).
[4] Weiss Z., Ďurovič S., Chmielová M., Krajíček J., Martinec P.: *Crystallochemistry and polytypism of micas*, Res. Report No. 67033, VVUÚ Ostrava — in Czech (1982).
[5] Mikloš D., Weiss Z.: *8th Conference on Clay Miner. and Petrology*, Teplice. 97 (1979).
[6] Backhaus K. O., Ďurovič S.: Clays and Clay Min. (in the press).
[7] Ďurovič S., Weiss Z., Backhaus K. O.: Clay and Clay Min. (in the press).
[8] Mikloš D.: CSc. Thesis, Inst. Inorg. Chem. Slovak Acad. Sci. ,Bratislava (1975).
[9] Ďurovič S., Weiss Z.: Silikáty *27*, 1 (1983).
[10] Dornberger-Schiff K.: Abh. Dtsch. Akad. Wiss. Berlin Kl. Chem. Geol. Biol. No. 3 (1964).
[11] Fichtner K.: Beitr. z. Algebra und Geometrie *6*, 71 (1977).
[12] Ďurovič S.: Fortschr. Mineral. *59*, 191 (1981).
[13] Weiss Z., Ďurovič S.: *Euroclay' 83*, Praha (submitted).
[14] Zvyagin B. B.: *Electron diffraction analysis of clay minerals*. Plenum Press, New York (1967).
[15] Zvyagin B. B., Vrublevskaya Z. V., Zhoukhlistov A. P., Sidorenko O. V., Soboleva S. V. Fedotov A. F.: *Vysokovoltnaya elektronographya v issledovanii sloistykh mineralov*. Nauka, Moskva 1979.

[16] Plancon A., Rousseaux F., Tchoubar D., Tchoubar C., Krinari G., Drits V. A.: J. Appl. Cryst. *15*, 509 (1982).
[17] Wiewióra A., Weiss Z., Krajíček J.: *Euroclay' 83*, Praha (submitted).
[18] Lee J. H., Guggenheim S.: Am. Mineral. *66*, 350 (1981).
[19] Rayner J. H., Brown G.: Clays and Clay Min. *21*, 103 (1973).
[20] Weiss Z., Krajíček J., Smrčok Ľ., Fiala J.: J. Appl. Cryst. *16*, 493 (1983).

POLYTYPISMUS PYROFYLITU A MASTKU

Část II. Klasifikace a rentgenografická identifikace MDO polytypů

Zdeněk Weiss, Slavomil Ďurovič*

Vědeckovýzkumný uhelný ústav, 716 07 Ostrava

**Ústav anorganickej chémie, Centrum chemického výskumu, Slovenská akadémia vied, 842 36 Bratislava*

MDO polytypy pyrofylitu a mastku byly podle jejich superpozičních struktur rozděleny na dvě subfamilie. Podle projekce struktury těchto polytypů na rovinu *YZ* byly tyto rozděleny do sedmi (u mastkové familie) a patnácti (u pyrofylitové famile) MDO grup. Tato geometrická klasifikace, která souvisí s difrakčním obrazem těchto minerálů, byla potvrzena systematickými výpočty rentgenových difrakčních obrazů všech odvozených MDO polytypů. Kromě toho umožnily provedené výpočty sestavení identifikačních diagramů pro určení subfamilie a MDO grupy, podle distribuce intenzit difrakcí $\pm 20l$ ($\pm 13l$) a $02l$. Tyto dvě charakteristiky dovolují určit jakýkoliv MDO polytyp. Zmíněná identifikace je založena na srovnání monokrystalových difrakčních dat s vypočítanými identifikačními diagramy. Částečná identifikace je také možná, použijeme-li práškové difrakční záznamy pořízené analýzou vzorku s náhodně orientovanými částicemi.

Obr. 1. Schematické znázornění vypočítaných hodnot $|F|^2$ (nejvyšší hodnota $|F|^2$ každé subfamilie je znázorněna největším kruhem) charakteristických difrakcí 20l pro MDO polytypy mastku a jejich klasifikace do subfamilií A a B. Indexace je vztažena k šestivrstevné ortogonální buňce. K výpočtu indexů u subfamilie A byla použita rovnice odpovídající mřížkové geometrii typu d) a u subfamilie B odpovídající mřížkové geometrii typu a) — viz. tab. III.

Obr. 2. Schematické znázornění vypočítaných hodnot $|F|^2$ (nejvyšší hodnota $|F|^2$ každé subfamilie je znázorněna největším kruhem) charakteristických difrakcí 20l pro MDO polytypy pyrofylitu a jejich klasifikace do subfamilií A a B. Indexace je vztažena k šestivrstevné ortogonální buňce. K výpočtu indexů u subfamilie A byla použita rovnice odpovídající mřížkové geometrii typu d) a u subfamilie B odpovídající mřížkové geometrii typu a) — viz. tab. III.

Obr. 3. Schematické znázornění vypočítaných hodnot $|F|^2$ (nejvyšší hodnota $|F|^2$ každé MDO grupy je znázorněna největším kruhem) charakteristických difrakcí 02l pro MDO polytypy mastku a jejich klasifikace do MDO grup I, II a III. Indexace je vztažena k šestivrstevné ortogonální buňce. Rovnice pro výpočet indexů jsou uvedeny v tab. III.

Obr. 4. Schematické znázornění vypočítaných hodnot $|F|^2$ (nejvyšší hodnota $|F|^2$ každé MDO grupy je znázorněna největším kruhem) charakteristických difrakcí 02l pro MDO polytypy mastku a jejich klasifikace pro MDO grup IV až VII. Indexace je vztažena k šestivrstevné ortogonální buňce. Rovnice pro výpočet indexů jsou uvedeny v tab. III.

Obr. 5. Schematické znázornění vypočítaných hodnot $|F|^2$ (nejvyšší hodnota $|F|^2$ každé MDO grupy je znázorněna největším kruhem) charakteristických difrakcí 02l pro MDO polytypy pyrofylitu a jejich klasifikace do MDO grup I, 1; I, 2; I, 3 a II, 1. Indexace je vztažena k šestivrstevné ortogonální buňce. Rovnice pro výpočet indexů jsou uvedeny v tab. III.

Obr. 6. Schematické znázornění vypočítaných hodnot $|F|^2$ (nejvyšší hodnota $|F|^2$ každé MDO grupy je znázorněna největším kruhem) charakteristických difrakcí 02l pro MDO polytypy pyrofylitu a jejich klasifikace do MDO grup III, 1; IV, 1 a IV, 2. Indexace je vztažena k šestivrstevné ortogonální buňce. Rovnice pro výpočet indexů jsou uvedeny v tab. III.

Obr. 7. Schematické znázornění vypočítaných hodnot $|F|^2$ (nejvyšší hodnota $|F|^2$ každé MDO grupy je znázorněna největším kruhem) charakteristických difrakcí 02l pro MDO polytypy pyrofylitu a jejich klasifikace do MDO grup IV, 3; V, 1; VI, 1 (VI, 3); VI, 2 a VII, 1 (VII, 2; VII, 3). Indexace je vzdálena k šestivrstevné ortogonální buňce. Rovnice pro výpočet indexů jsou uvedeny v tab. III.

Obr. 8. Srovnání charakteristických hodnot $|F(20l)|^2$ a $|F(02l)|^2$ vypočítaných na základě strukturních dat, které publikovali Lee a Guggenheim [18] — (obs) s teoretickými hodnotami vypočítanými pro MDO polytyp $1Tc_A$ — II, 1 pyrofylitu — (calc). Hodnoty $|F|^2$ jsou normalizovány vzhledem k nejsilnější difrakci. Indexace je vztažena ke skutečné jednovrstevné buňce.

Obr. 9. Srovnání charakteristických hodnot $|F(20l)|^2$ a $|F(02l)|^2$ vypočítaných na základě strukturních dat, které publikovali Rayner a Brown [19] *— (obs) s teoretickými hodnotami vypočítanými pro MDO polytyp $1Tc_A$ — II mastku — (calc). Hodnoty $|F|^2$ jsou normalizovány vzhledem k nejsilnější difrakci. Indexace je vztažena ke skutečné jednovrstevné buňce.*

Obr. 10. Vypočítané rentgenové práškové difrakční záznamy tří MDO polytypů mastku (experimentální uspořádání : difraktometr, záření Cu, náhodná orientace částic ve studovaném vzorku):

a) $\left|\begin{matrix} e\,.\,e \\ 3\ \ 3 \end{matrix}\right|$ $(1M_A - I)$

b) $\left|\begin{matrix} e\,.\,e \\ 5\ \ 1 \end{matrix}\right|$ $(1Tc_A - II)$

c) $\left|\begin{matrix} u\,.\,u\,.\,u\,.\,u \\ 0\ \ 4\ \ 0\ \ 2 \end{matrix}\right|$ $(2M_A - IV)$

ПОЛИТИПИЯ ПИРОФИЛЛИТА И ТАЛЬКА

Часть II. Классификация и рентгенографическая идентификация МДО политипов

Зденек Вейсс, Славомил Дюрович*

Научно-исследовательский институт, 716 07 Острава
**Институт неорганической химии, Центр химического исследования Словацкая Академия Наук, 842 36 Братислава*

МДО политипы пирофиллита и талька были разделены в два субсемейства, отвечающие их суперпозиционным структурам. В соответствии с проекцией структуры этих политипов в плоскость YZ, данные политипы были разделены в семь МДО групп (в случае семейства талька) и пятнадцать МДО групп (в случае семейства пирофиллита). Такая геометрическая классификация, отвечающая диффракционным спектрам этих минералов, была подтверждена систематическими расчетами рентгеновских диффракционных спектров всех выведенных МДО политипов. Кроме того, на основе выше указанных расчетов было возможно составить диаграммы для идентификации субсемейства и МДО группы в зависимости от распределения интенсивности диффракций $\pm 20l$ ($\pm 13l$) и $02l$. Эти две характеристики позволяют провести идентификацию любового МДО политипа. Идентификация основана на сравнении монокристаллических диффракционных данных с расчетными данными указанными в идентификационных диаграммах. Возможна также частичная идентификация в том случае, если применяются порошковые диффракционные спектры, полученные путем анализа пробы со случайно ориентированными частицами.

Рис. 1. Схематическое изображение расчетных данных $|F|^2$ (высшая величина $|F|^2$ каждого субсемейства обозначена большим кольцом) соответствующих характеристическим диффракциям $20l$ МДО политипов талька и их разделение в субсемейства А и Б. Индексация относится к шестислоистой прямоугольной ячейке. Для расчета индексов субсемейства А была применена формула отвечающая геометрии решетки типа d) и для расчета индексов субсемейства Б геометрия решетки типа a) (смотри таб. III).

Рис. 2. Схематическое изображение расчетных данных $|F|^2$ (высшая величина $|F|^2$ каждого субсемейства обозначена большим кольцом) соответствующих характеристическим диффракциям $20l$ МДО политипов пирофиллита и их разделение в субсемейства А и Б. Индексация относится к шестислоистой прямоугольной ячейке. Для расчета индексов субсемейства А была применена формула отвечающая геометрии решетки типа d) и для расчета индексов субсемейства Б геометрия решетки типа a) (смотри таб. III).

Рис. 3. Схематическое изображение расчетных данных $|F|^2$ (высшая величина $|F|^2$ каждой МДО группы обозначена большим кольцом) соответствующих характеристическим диффракциям 02l МДО политипов талька и их разделение в МДО группы I, II, и III. Индексация относится к шестислоистой прямоугольной ячейке. Формулы для расчета индексов указаны в таблице III.

Рис. 4. Схематическое изображение расчетных данных $|F|^2$ (высшая величина $|F|^2$ каждой МДО группы обозначена большим кольцом) соответствующих характеристическим диффракциям 02l МДО политипов талька и их разделение в МДО группы IV—VII. Индексация относится к шестислоистой прямоугольной ячейке. Формулы для расчета индексов указаны в таб. III.

Рис. 5. Схематическое изображение расчетных данных $|F|^2$ (высшая величина $|F|^2$ каждой МДО группы обозначена большим кольцом) соответствующих характеристическим диффракциям 02l МДО политипов пирофиллита и их разделение в МДО группы I, 1; I, 2; I, 3 и II, 1. Индексация относится к шестислоистой прямоугольной ячейке. Формулы для расчета индексов указаны в таб. III.

Рис. 6. Схематическое изображение расчетных данных $|F|^2$ (высшая величина $|F|^2$ каждой МДО группы обозначена большим кольцом) соответствующих характеристическим диффракциям 02l МДО политипов пирофиллита и их разделение в МДО группы III, 1; IV, 1 и IV, 2. Индексация относится к шестислоистой прямоугольной ячейке. Формулы для расчета индексов указаны в таб. III.

Рис. 7. Схематическое изображение расчетных данных $|F|^2$ (высшая величина $|F|^2$ каждой МДО группы обозначена большим кольцом) соответствующих характеристическим диффракциям 02l МДО политипов пирофиллита и их разделение в МДО группы IV, 3; V, 1; VI, 1 (VI, 3); VI, 2 и VII, 1 (VII, 2; VII, 3). Индексация относится к шестислоистой прямоугольной ячейке. Формулы для расчета индексов указаны в таб. III.

Рис. 8. Сравнение характеристических величин $|F(20l)|^2$ и $|F(02l)|^2$ полученных расчетом из структурных данных, опубликованных в [18] — (obs), причем теоретические величины были исчислены для МДО политипа 1Tc—II, 1 пирофиллита — (calc). Величины $|F|^2$ нормализированны в отношении к самой интенсивной диффракции. Индексация относится к настоящей однослоистой ячейке.

Рис. 9. Сравнение характеристических величин $|F(20l)|^2$ и $|F(02l)|^2$ полученных расчетом из структурных данных, опубликованных в [19] — (obs), причем теоретические величины были исчислены для МДО политипа $1T_A$-II талька — (calc). Величины $|F|^2$ нормализированы в отношении к самой интенсивной диффракции. Индексация относится к настоящей однослоистой ячейке.

Рис. 10. Расчетные рентгеновские порошковые диффракционные спектры трех МДО политипов талька (условия эксперимента: диффрактометр, излучение Cu, случайная ориентация частиц в изучаемой пробе):

а) $\left|\begin{matrix} e & . & e \\ 3 & 3 \end{matrix}\right|$ $(1M_A\text{-}I)$

б) $\left|\begin{matrix} e & . & e \\ 5 & 1 \end{matrix}\right|$ $(1Tc_A\text{-}II)$

в) $\left|\begin{matrix} u & . & u & . & u & . & u \\ 0 & & 4 & & 0 & & 2 \end{matrix}\right|$ $(2M_A\text{-}IV)$
